Combination of Functional Magnetic Resonance Imaging and Histopathologic Analysis to Evaluate Interstitial Fibrosis in Kidney Allografts

Wei Wang,[1] Yuanmeng Yu,[2] Jiqiu Wen,[3] Mingchao Zhang,[3] Jinsong Chen,[3] Dongrui Cheng,[3] Longjiang Zhang,[2,4] and Zhihong Liu[1,3]

Abstract

Background and objectives Recent developments indicated that functional magnetic resonance imaging (MRI) could potentially provide noninvasive assessment of kidney interstitial fibrosis in patients with kidney diseases, but direct evidence from histopathology is scarce. We aimed to explore the diagnostic utilities of functional MRI for the evaluation of kidney allograft interstitial fibrosis.

Design, setting, participants, & measurements We prospectively examined 103 kidney transplant recipients who underwent for-cause biopsies and 20 biopsy-proven normal subjects with functional MRI. Histomorphometric analyses of interstitial fibrosis and peritubular capillary densities were performed on digitally scanned Masson's trichrome- and CD34-stained slides, respectively. The performances of functional MRI to discriminate interstitial fibrosis were assessed by calculating the area under the curve using receiver-operating characteristic curve.

Results Main pathologic findings in this single-center cohort were representative of common diagnostic entities in the kidney allografts, with rejection (32%) and glomerulonephritides (31%) accounting for the majority of diagnoses. Apparent diffusion coefficient from diffusion-weighted imaging correlated with interstitial fibrosis (ρ=−0.77; P<0.001). Additionally, decreased arterial spin labelings were accompanied by peritubular capillary density reductions (r=0.77; P<0.001). Blood oxygen level–dependent (BOLD) imaging demonstrated cortical hypoxia with increasing interstitial fibrosis (ρ=0.61; P<0.001). The area under the curve for the discrimination of ≤25% versus >25% interstitial fibrosis and ≤50% versus >50% interstitial fibrosis were 0.87 (95% confidence interval [95% CI], 0.79 to 0.93) and 0.88 (95% CI, 0.80 to 0.93) by apparent diffusion coefficient, 0.92 (95% CI, 0.85 to 0.97) and 0.94 (95% CI, 0.87 to 0.98) by arterial spin labeling, 0.81 (95% CI, 0.72 to 0.88) and 0.86 (95% CI, 0.78 to 0.92) by perfusion fraction, 0.79 (95% CI, 0.69 to 0.87) and 0.85 (95% CI, 0.76 to 0.92) by BOLD imaging, respectively.

Conclusions Functional MRI measurements were strongly correlated with kidney allograft interstitial fibrosis. The performances of functional MRI for discriminating ≤50% versus >50% interstitial fibrosis were good to excellent.

CJASN 14: 1372–1380, 2019. doi: https://doi.org/10.2215/CJN.00020119

[1]National Clinical Research Center of Kidney Diseases, Jinling Clinical Medical College of Nanjing Medical University, Nanjing, China; [2]Department of Medical Imaging, Jinling Hospital, Clinical School of Southern Medical University, Nanjing, China; [3]National Clinical Research Center of Kidney Diseases, Nanjing University School of Medicine, Nanjing, China; and [4]Department of Medical Imaging, Jinling Hospital, Medical School of Nanjing University, Nanjing, China

Correspondence: Prof. Zhihong Liu, National Clinical Research Center of Kidney Diseases, Jinling Clinical Medical College of Nanjing Medical University, 305 East Zhongshan Road, Xuanwu District, Nanjing, Jiangsu 210002, China, or Dr. Longjiang Zhang, Department of Medical Imaging, Jinling Hospital, Medical School of Nanjing University, Nanjing, Jiangsu 210002, China. E-mail: liuzhihong@nju.edu.cn or kevinzhlj@163.com

Introduction

The process of interstitial fibrosis, which is characterized histologically by extracellular collagen deposition, tubular atrophy, and peritubular capillary rarefaction, is an essential converging pathway for a variety of insults that incur irreversible kidney allograft injuries. Interstitial fibrosis, oxygenation, and peritubular capillary integrity have been demonstrated to be major determinants for the progression of chronic injury and thus kidney survival (1). It is desirable that these fibrosis-related parameters can be noninvasively determined that obviates disadvantages of invasiveness and sampling bias associated with kidney allograft biopsy.

Previous studies (2,3) have sought extensively to identify serum/urinary biomarkers to assess kidney interstitial fibrosis noninvasively. An alternative or complementary approach is through functional magnetic resonance imaging (MRI), which has been shown to be able to quantify various pathophysiologic parameters *in vivo* that are otherwise unobtainable in humans (4). Despite these putative advantages, the relationships between *in vivo* functional MRI parameters and interstitial fibrosis have been scarcely appraised. Obviously, validations of functional MRI against histopathology could facilitate its translation to an invaluable tool for the multilateral assessment of kidney interstitial fibrosis in clinical practice.

Blood oxygen level–dependent (BOLD) imaging is a well established technique that detects altered deoxyhemoglobin level as a surrogate marker of tissue oxygenation (5,6). Diffusion-weighted imaging quantifies tissue water molecule free movement by calculating the apparent diffusion coefficient, which is reportedly restricted with the extracellular deposition

of collagen and microstructure disorganization (7). Arterial spin labeling, which tags inflowing blood as an endogenous contrast, has been shown to be a robust and reproducible technique to measure tissue microvascular perfusion (8). Preliminary studies have shown decreased arterial spin labeling readings with deteriorating functions of the native kidneys with CKD (9) and kidney transplants (10).

This study aimed to validate these novel functional MRI measurements against kidney allograft biopsy findings to establish radiologic–histopathologic correlations, which could potentially be applied clinically to assess interstitial fibrosis *in vivo* in the future.

Materials and Methods

Patients

In this single-center, prospective study conducted from September 2016 to September 2018, we selected adult kidney transplant recipients who underwent indication biopsies and normal kidney transplant recipients who underwent surveillance biopsies to undergo functional MRI. All adult patients with biopsy results were eligible for functional MRI examinations. Exclusion criteria were the presence of MRI-incompatible devices, claustrophobia, and patient refusal. Eligible patients who did not meet the exclusion criteria were chosen when an MRI slot was available (generally one to two examinations per week). Only kidneys known to be procured with the consents of the donors or their family members were included in the final analysis. Data from patients with unknown sources of transplanted kidneys were excluded from final analysis. The study flowchart is shown in Supplemental Figure 1. Biopsies designated as normal were defined as having a Banff interstitial fibrosis plus inflammation score of 0 and no evidence of a specific disease process. Functional MRI examinations were performed within 1 week after biopsy. The CKD Epidemiology Collaboration equation was applied to calculate the eGFR. All the patients included in the final analysis underwent kidney transplantation that was approved by the Institutional Review Board of Jinling Hospital, Nanjing University School of Medicine and conformed to the tenets of the Declaration of Helsinki. Written informed consents were collected from all patients before performing allograft biopsies. Functional MRI is a well established technique at our hospital, thus no additional proven document from the Institutional Review Board for performing this examination was obtained.

MRI Protocols

Selected patients were instructed to fast for at least 6 hours before MRI examinations, which were performed on a 3.0 Tesla clinical imager (Discovery MR750; General Electric, Milwaukee, WI). All relevant imaging parameters are summarized in Supplemental Table 1. First, coronal T1- and axial T2-weighted images covering the entire allograft were acquired for anatomic characterization. Coronal BOLD images were then obtained with kidney allograft hilum located at the center, using a 12-echo, multiplanar, fast gradient echo sequence. Four coronal sections of kidneys were acquired with a 5-mm section thickness and a 5-mm intersection gap during 15-second breath holds (11). Axial, multisection, respiration-triggered, echo-planer diffusion-weighted imaging was performed with a panel of ten nonzero gradient b values (10, 30, 50, 70, 100, 150, 200, 400, 800, and 1000 s/mm^2) that were applied in three orthogonal directions and subsequently averaged to minimize the effects of diffusion anisotropy. Kidney allograft perfusion was measured using a prototype three-dimensional arterial spin labeling sequence with the pseudocontinuous arterial spin labeling scheme and spiral K space filling, as previously reported (12). MRI examinations were repeated in the presence of technical failures or image artifacts that distorted image quality to ensure that the acquired images were analyzable.

Functional MRI Image Analyses

MRI raw data were transferred to Advantage 4.6 Functool Workstation (General Electronic) for subsequent analyses. All images were analyzed by the first author, and regions of interests (ROIs) were confirmed by an experienced radiologist (L.Z.). Both were blinded to the clinical and pathologic results to eliminate potential biases. Areas/slices with cysts, hemorrhages, heterogeneous signal intensities, or vascular structures were excluded when delineating ROIs.

Cortical R2* values were determined by placing five to eight ellipsoid ROIs (approximately 20–50 mm^2 each) manually on the cortex on the coregistered T2-weighted images that yielded optimal cortical-medullary differentiation, and then copying ROIs to the corresponding parametric map of R2* (6). R2* was calculated by fitting an exponential curve to individual voxels over the echo times. Mean cortical R2* values were calculated as the mean values of the ROIs.

Diffusion-weighted imaging signals were analyzed by fitting monoexponential and biexponential models to the signal decay (13). Apparent diffusion coefficient was derived by fitting all 11 b values to the monoexponential model. Perfusion fraction was generated using intravoxel incoherent motion model. Data sets from three cortical ROIs covering the entire cortex on three consecutive perihilar slices were averaged to obtain a single data set for subsequent analysis.

Quantitative kidney allograft perfusion were calculated using the Arterial Spin Labeling toolkit from Functool software package (9). Labeling efficiency was set to 0.8, partition coefficient was 0.9, and T1 of blood at 3.0 Tesla was set to 1.6 ms. Three ROIs covering the entire kidney cortex each were placed manually on three consecutive perihilar slices, the readings of which were subsequently averaged to represent allograft perfusion.

Functional MRI images from 20 patients were randomly selected and analyzed independently by an in-house abdominal radiologist (Y.Y.) to test the measurement reproducibility of various functional MRI parameters by calculating the intraclass correlation coefficients.

Morphologic Evaluation and Morphometry

Pathologic diagnoses and elementary lesions scoring were performed by an experienced nephropathologist (M.Z.) according to the Banff 2015 schema (14) without referring to functional MRI results. All stained light microscopic slides were digitally scanned using a digital pathology platform (Aperio Scanscope XT Turbo Scanner; Leica,

Table 1. Patient demographics, clinical features, laboratory characteristics, and pathology findings in 123 patients who underwent functional magnetic resonance imaging and allograft biopsy

Characteristics/Findings	Allograft Injury Group (*n*=103)	Normal Control Group (*n*=20)
Donor age, yr, median (IQR)	51 (43–56)	50 (45–52)
Donor sex, male, *n* (%)	40 (39)	10 (50)
Recipient age, yr, mean (±SD)	38±10	35±9
Recipient sex, male, *n* (%)	73 (71)	16 (80)
Causes of ESKD		
Unknown, *n* (%)	74 (72)	15 (75)
Glomerulonephritides, *n* (%)	21 (20)	4 (20)
Other, *n* (%)	8 (8)	1 (5)
Transplant type		
Living donor kidney transplant, *n* (%)	44 (43)	9 (45)
Deceased donor kidney transplant, *n* (%)	59 (57)	11 (55)
Immunosuppressive regimens		
Pre+MMF+FK506, *n* (%)	74 (72)	17 (85)
Pre+MMF+CsA, *n* (%)	13 (13)	2 (10)
Other, *n* (%)	16 (15)	1 (5)
Serum creatinine, mg/dl, median (IQR)	1.9 (1.4–2.6)	1.2 (1.0–1.3)
eGFR, ml/min per 1.73 m^2, median (IQR)	47 (21–61)	81 (71–85)
Proteinuria, g/24 h, median (IQR)	0.5 (0.3–1.5)	0.2 (0.1–0.3)
Hemoglobin level, g/dl, mean (±SD)	11.5±2.2	13.9±2.5
Concomitant antihypertensives		
Renin-angiotensin blockers, *n* (%)	34 (33)	3 (15)
Calcium channel blockers, *n* (%)	58 (56)	10 (50)
β-Blockers, *n* (%)	31 (30)	9 (45)
Diuretics, *n* (%)	4 (4)	0 (0)
α-Receptor antagonists, *n* (%)	9 (9)	2 (10)
Main pathologic diagnoses in the allograft injury group	IgA nephropathy (*n*=22); chronic active AMR (*n*=17); IF/TA (*n*=10); acute AMR (*n*=6); BK virus nephropathy (*n*=6); CNI toxicity (*n*=6); acute mixed rejection (*n*=5); FSGS (*n*=5); donor-derived changes (*n*=5); idiopathic thrombotic microangiopathy (*n*=5); T cell–mediated rejection (*n*=5); glomerulosclerosis (*n*=3); transplant glomerulopathy suspicious for chronic AMR (*n*=3)[a]; MN (*n*=3); PGNMID (*n*=1); MPGN (*n*=1)	

IQR, interquartile range; Pre, prednisone; MMF, mycophenolate mofetil; FK506, tacrolimus; CsA, cyclosporine A; AMR, antibody-mediated rejection; IF/TA, interstitial fibrosis/tubular atrophy; CNI, calcineurin inhibitor; MN, membranous nephropathy; PGNMID, proliferative GN with monoclonal IgG deposits; MPGN, membranoproliferative glomerulonephritis.
[a]In these three cases, both glomerulitis (g) and peritubular capillaritis (ptc) were present and g+ptc≥2, in addition to the histologic finding of glomerular capillary duplication. However, panel reactive antibody screening was negative, making the diagnosis of antibody-mediated rejection likely but not definitive according to the criteria outlined in the 2015 Banff Schema.

Wetzlar, Germany). An annotation layer covering the entire sampled cortex area was created manually, in which glomeruli and interstitial large vessels were excluded from analysis.

Interstitial fibrosis quantification was done on Masson trichrome–stained slides by calculating the percentage of brilliant blue areas using the Colocalization algorithm (version 9; Aperio Technologies, Inc.) (15), which uses the deconvolution method to separate the stains and classifies each pixel according to the number of stains present. The red, green, and blue components were (*1*) 0.655, 0.664, and 0.36, respectively, for color; (*2*) 0.155, 0.748, and 0.645, respectively, for color; and (*3*) 0.938, 0.245, and 0.247, respectively, for color.

We performed CD34 immunostaining to highlight the interstitial capillaries. The number of peritubular capillaries were calculated by first creating an annotation layer in a manner similar to that described for interstitial fibrosis quantification, followed by analysis using the Aperio Microvessel algorithm (Aperio Technologies, Inc.), as exemplified in Supplemental Figure 2. The outputs were standardized and reported as peritubular capillary density (peritubular capillary number in a given tubulointerstitium).

In line with the Banff 2015 classification (14), calculated interstitial fibrosis was categorized into Banff interstitial fibrosis score 0 (interstitial fibrosis ≤5%), interstitial fibrosis score 1 (>5% to ≤25%), interstitial fibrosis score 2 (>25% to ≤50%), or interstitial fibrosis score 3 (>50%).

Statistical Analyses

The significance of the continuous parameters was determined by *t* test or the Mann–Whitney *U* test for two groups. Comparisons of functional MRI data from subgroups with different Banff interstitial fibrosis scores were performed with one-way ANOVA or Kruskal–Wallis test, as appropriate. The *post-hoc* Tukey test was used to compare individual groups when the ANOVA result was significant. Pearson or Spearman correlation was used to evaluate the correlations between functional MRI parameters and histomorphometry variables, as appropriate. The diagnostic performances of functional MRI measurements for the discrimination of various Banff interstitial fibrosis scores were assessed by calculating the area under the curve

(AUC) using receiver-operating characteristic curve. For BOLD results that were unavailable in 13 patients, all statistical analysis were performed using data from those with available BOLD results. Given that anemia has been reported to confound BOLD and arterial spin labeling measurement (16,17), we in a sensitivity analysis calculated the correlations between these functional MRI measurements and histomorphology variables using partial correlation that controlled for hemoglobin level. A two-sided P value <0.05 was deemed to be statistically significant.

Results

Patient Demographics, Clinical Features, Laboratory Characteristics, and Pathology Findings

Functional MRI data from 103 patients (allograft injury group) who underwent for-cause biopsies, and 20 patients (normal control group) who underwent surveillance biopsies were analyzed. These patients underwent kidney transplantation between 2007 and 2018 with a median time of 19 months (interquartile range [IQR], 7–57 months) post-transplant. Specific indications for for-cause biopsy were serum creatinine elevation (56%, 58/103) alone, proteinuria (15%, 15/103) alone, and both serum creatinine elevation and proteinuria (29%, 30/103). No statistically significant differences were observed between these two groups with regard to donor demographics, recipient age, sex, kidney transplant type, immunosuppressive regimens used, and concomitant antihypertensive usage (Table 1). Unsurprisingly, mean hemoglobin level of the allograft injury group was much lower than that of the normal control group (11.5±2.2 g/dl versus 13.9±2.5 g/dl; $P<0.001$). Causes of ESKD were overwhelmingly unknown in both groups.

Main pathologic findings in the allograft injury group were representative of common diagnostic entities in the kidney allografts, with allograft rejection (32%, 33/103) and glomerulonephritides (31%, 32/103) accounting for the majority of diagnoses. Median interstitial fibrosis of the allograft injury group was 23% (IQR, 10%–45%).

Arterial spin labeling and diffusion-weighted imaging were acquired for all 123 patients. BOLD results were unavailable in three patients in the normal control group and ten patients in the allograft injury group, all of whom were examined during the initial period of this study when BOLD has not been implemented in the MRI machine.

Evaluation of Interstitial Fibrosis with Apparent Diffusion Coefficient

Cortical apparent diffusion coefficient was significantly decreased in the allograft injury group than normal control group (1.98 [IQR,1.80–2.17]$\times10^{-3}$mm^2/s versus 2.28 [IQR, 2.16–2.35]$\times10^{-3}$mm^2/s; $P<0.001$; Figure 1A). An ANOVA test among patients with different Banff interstitial fibrosis scores was significant, and a *post hoc* Tukey test suggested that compared with normal control group, a significantly reduced mean apparent diffusion coefficient value could even be observed in patients in the allograft injury group with Banff interstitial fibrosis score 1. Apparent diffusion coefficient was significantly inversely correlated with interstitial fibrosis (rho=−0.77; $P<0.001$; Figure 1, B–D) for patients with allograft injury.

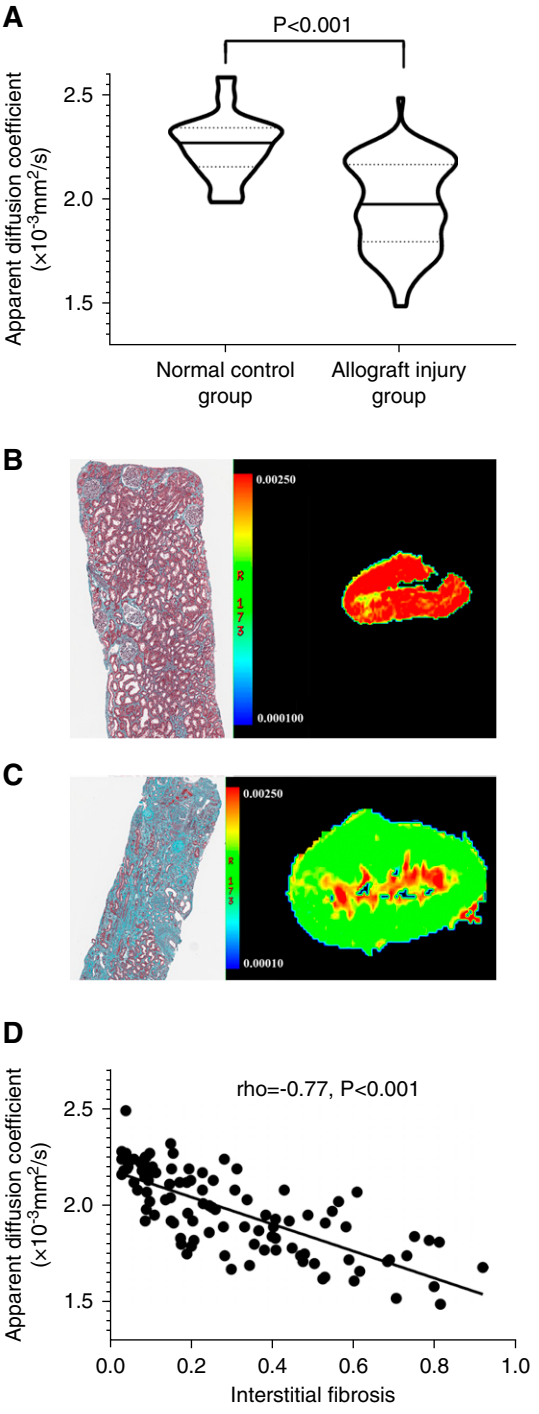

Figure 1. | Assessment of kidney allograft interstitial fibrosis with diffusion-weighted imaging. (A) Violin plot demonstrating that apparent diffusion coefficient in the normal control group is significantly higher than in the allograft injury group. The solid line represents the median, and the dotted lines represent the 25% and 75% IQR. (B and C) Representative examples of water molecular movement restriction with increasingly severe interstitial fibrosis. (B) The allograft hue turns from deep red in a normal allograft (Masson) to (C) green in a dysfunctional allograft with severe (>50%) interstitial fibrosis (Masson). (D) Cortical apparent diffusion coefficients were inversely correlated with interstitial fibrosis (rho=−0.77; $P<0.001$) in patients with allograft injury. Original magnification, ×100 in (B) and (C).

Assessing Peritubular Capillary Density with Functional MRI-Derived Perfusion Parameters

Peritubular capillary density was drastically reduced in the allograft injury group compared with the normal control group (266±79/mm^2 versus 334±52/mm^2; $P<0.001$; Supplemental Figure 3A), and it was negatively associated with interstitial fibrosis in the allograft injury group (rho=−0.64; $P<0.001$; Supplemental Figure 3B). Functional MRI measurement showed significantly decreased allograft perfusion in the allograft injury group compared with normal control group (Figure 2, A and B). Arterial spin labeling was significantly correlated with peritubular capillary density ($r=0.77$; $P<0.001$; Figure 2C). Similar association was also observed for cortical perfusion fraction ($r=0.59$; $P<0.001$). In fact, allograft perfusion as detected by arterial spin labeling correlated with microcirculatory perfusion as determined by perfusion fraction ($r=0.59$; $P<0.001$; Figure 2D).

BOLD Evaluation of Kidney Allograft Cortical Oxygenation

Cortical R2* was significantly higher in patients with allograft injury than in normal controls (17.8 [IQR, 16.5–20.1] Hz versus 15.6 [IQR, 15.1–16.8] Hz; $P<0.001$; Figure 3A). Cortical R2* demonstrated significant correlation with interstitial fibrosis (rho=0.61; $P<0.001$; Figure 3B) and allograft perfusion assessed by arterial spin labeling (rho=−0.52; $P<0.001$). Patients with Banff interstitial fibrosis score 2 and score 3 had significantly higher cortical R2* than normal controls (Figure 3, C and D).

In the sensitivity analysis, the correlation between cortical R2* and interstitial fibrosis after adjusting for hemoglobin level was rho=0.58 ($P<0.001$). Arterial spin labeling was also significantly correlated with peritubular capillary density after controlling for hemoglobin level ($r=0.75$; $P<0.001$).

Performances of Functional MRI Measurements for the Identification of Interstitial Fibrosis among Kidney Transplant Patients with Allograft Injury

Results are shown in Table 2. For differentiating both ≤25% versus >25% interstitial fibrosis and >50% versus ≤50% interstitial fibrosis, the diagnostic performances of apparent diffusion coefficient and arterial spin labeling were good to excellent (all AUC ≥0.87). The diagnostic performances of perfusion fraction and BOLD for discriminating >50% versus ≤50% interstitial fibrosis were also good, with AUCs of 0.86 (95% confidence interval [95% CI], 0.78 to 0.92) and 0.85 (95% CI, 0.76 to 0.92), respectively. Nevertheless, perfusion fraction and BOLD differentiated ≤25% versus >25% interstitial fibrosis with AUCs of only 0.81 (95% CI, 0.72 to 0.88) and 0.79 (95% CI, 0.69 to 0.87), respectively. Noticeably, the AUCs of eGFR and all functional MRI parameters for the differentiation of >50% versus ≤50% interstitial fibrosis were comparable. However, the AUC for the discrimination of ≤25% versus >25% interstitial fibrosis by eGFR was statistically higher than those by perfusion fraction ($P=0.01$) and cortical R2* ($P=0.007$).

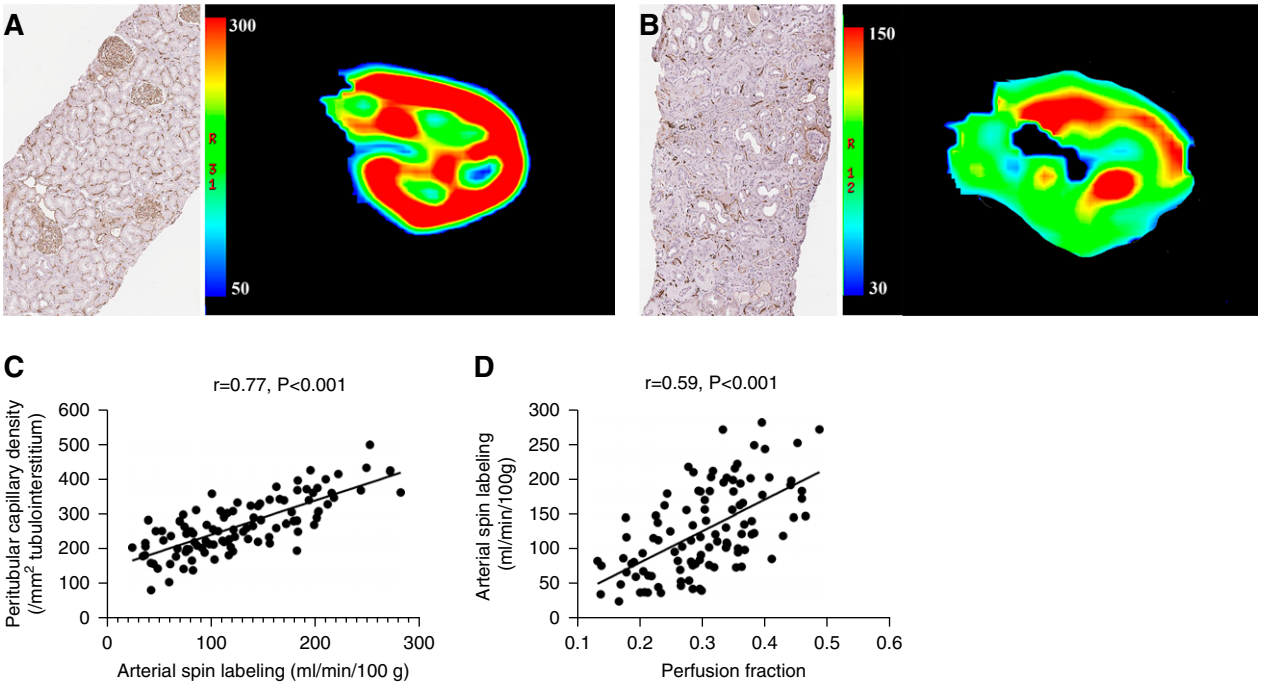

Figure 2. | Assessment of allograft peritubular capillary density with functional MRI-based perfusion quantification. (A and B) Compared with normal allografts (A) with well preserved peritubular capillaries, allografts with severe interstitial fibrosis (B) had peritubular capillary rarefaction and significantly lower allograft perfusion, as suggested by the reduced peritubular capillary density (CD34) and lower arterial spin labeling readings, respectively, in (B) than in (A) (Original magnification, ×40). (C) Allograft arterial spin labeling readings were significantly correlated with peritubular capillary density in the allograft injury group ($r=0.77$; $P<0.001$). (D) Arterial spin labeling readings were significantly correlated with cortical perfusion fraction calculated from diffusion-weighted imaging ($r=0.59$; $P<0.001$).

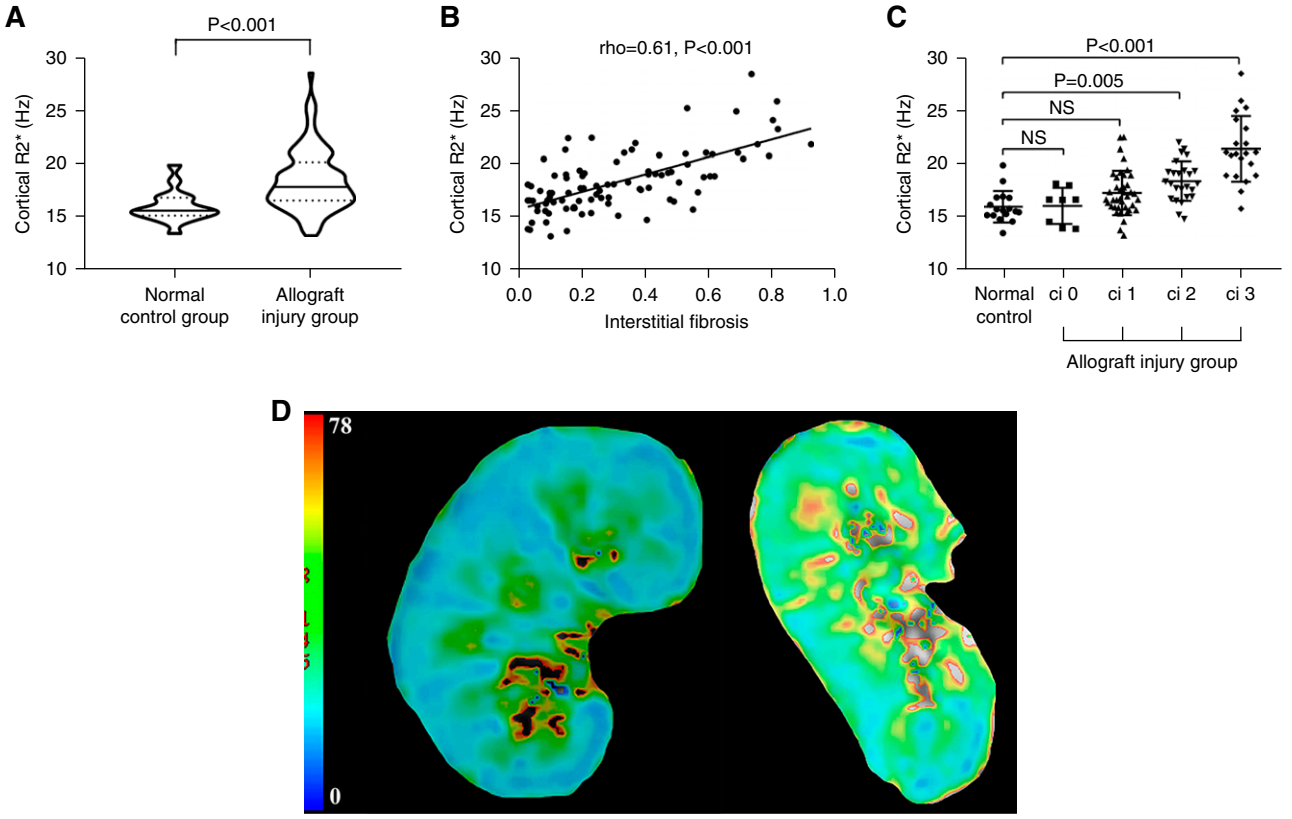

Figure 3. | **BOLD imaging evaluation of normal allografts and patients with allograft injury.** (A) Violin plot demonstrating that the median cortical R2* is significantly higher in the allograft injury group than in the normal control group. The solid line represent the median, whereas the dotted lines represented the 25% and 75% IQR. (B) Cortical R2* was correlated significantly with interstitial fibrosis in patients with allograft injury (rho=0.61; $P<0.001$). (C) One-way ANOVA with *post hoc* Tukey test suggested that the mean cortical R2* was significantly higher in allografts with moderate (>25% to ≤50%) and severe (>50%) fibrosis than in normal controls. (D) Representative example of kidney hypoxia (increased R2*) in allografts with severe fibrosis (right) compared with a normal allograft (left). ci, interstitial fibrosis score.

Interobserver Variability of Functional MRI Measurement

The intraclass correlation coefficients were 0.88 (95% CI, 0.73 to 0.95) for cortical R2*, 0.96 (95% CI, 0.90 to 0.98) for apparent diffusion coefficient, 0.83 (95% CI, 0.63 to 0.93) for perfusion fraction, and 0.98 (95% CI, 0.94 to 0.99) for arterial spin labeling.

Discussion

Although assessment of interstitial fibrosis by kidney biopsy remains the gold standard in clinical trials and practice, this procedure suffers from sampling variabilities and its invasiveness prevented from repeated performance. Preliminary studies in animal models and humans have shown promising results for functional MRI to be used to evaluate kidney function (6,9,10). Regrettably, the majority of published studies lacked histopathologic examinations, which are nevertheless critical for the validity of functional MRI to be used in a clinical setting. This cross-sectional study presents the application of functional MRI to evaluate salient pathophysiologic processes with regard to interstitial fibrosis in patients with kidney allograft injury, using biopsy as the reference standard. The results indicate that functional MRI can be used to evaluate kidney allograft interstitial fibrosis with a solid histopathologic basis.

Prior studies in the native kidneys have consistently demonstrated that apparent diffusion coefficient correlated with kidney function and interstitial fibrosis (7,10). We further extended and validated this technique to the kidney transplants in this study that concluded with a clear correlation between apparent diffusion coefficient and interstitial fibrosis, which is compatible with the only study in the kidney allografts that reported that diffusion-weighted imaging could allow determination of the severity of pathologic changes (18). Kidney interstitial fibrosis is an irreversible process that is accompanied by interstitial inflammatory cell infiltration, myofibroblast proliferation, and tissue microstructural disorganization, which can be detected by diffusion-weighted imaging that is particularly sensitive to water molecule free movement restriction.

Peritubular capillary rarefaction and remodeling have been identified as the hallmark for fibrosis progression in CKD and allograft injury (19). Quantification of peritubular capillary density would likely provide valuable information regarding fibrosis severity and allograft outcome. There are, to our knowledge, limited imaging techniques reported for noninvasive assessment of kidney microvasculature alterations. Ehling *et al.* (20) reported that functional *in vivo* microcomputed tomography imaging could allow for accurate and visually direct assessment of vessel

Table 2. Performances of eGFR and functional magnetic resonance imaging measurements for the differentiation of ≤25% versus >25% interstitial fibrosis and >50% versus ≤50% interstitial fibrosis among kidney transplant patients with allograft injury

Measurements	Correlations with Interstitial Fibrosis	≤25% versus >25% Interstitial Fibrosis				>50% versus ≤50% Interstitial Fibrosis			
		Cutoff	AUC (95% CI)	Sensitivity (95% CI)	Specificity (95% CI)	Cutoff	AUC (95% CI)	Sensitivity (95% CI)	Specificity (95% CI)
Apparent diffusion coefficient	rho=−0.77; $P<0.001$	1.99×10^{-3}mm^2/s	0.87 (0.79 to 0.93)	76% (62% to 87%)	84% (70% to 93%)	1.91×10^{-3}mm^2/s	0.88 (0.80 to 0.93)	86% (64% to 97%)	72% (61% to 81%)
Arterial spin labeling	rho=−0.83;; $P<0.001$	101 ml/min per 100 g	0.92 (0.85 to 0.97)	94% (85% to 99%)	78% (63% to 88%)	82.9 ml/min per 100 g	0.94 (0.87 to 0.98)	95% (76% to 99.9%)	87% (77% to 93%)
Perfusion fraction	rho=−0.66 $P<0.001$	0.299	0.81 (0.72 to 0.88)[a]	76% (62% to 87%)	78% (63% to 88%)	0.285	0.86 (0.78 to 0.92)	91% (70% to 99%)	72% (61% to 81%)
BOLD	rho=0.61; $P<0.001$	18.10 Hz	0.79 (0.69 to 0.87)[b]	79% (64% to 89%)	72% (57% to 84%)	18.14 Hz	0.85 (0.76 to 0.92)	91% (70% to 99%)	69% (58% to 80%)
eGFR[c]	rho=−0.79; $P<0.001$	38 ml/min per 1.73 m^2	0.91 (0.84 to 0.96)	91% (80% to 97%)	78% (63% to 88%)	38 ml/min per 1.73 m^2	0.91 (0.84 to 0.96)	95% (76% to 99.9%)	72% (61% to 81%)
eGFR[d]	rho=−0.79; $P<0.001$	38 ml/min per 1.73 m^2	0.93 (0.85 to 0.97)	89% (77% to 97%)	83% (69% to 92%)	38 ml/min per 1.73 m^2	0.90 (0.82 to 0.95)	95% (76% to 99.9%)	68% (56% to 79%)

eGFR calculated by the CKD Epidemiology Collaboration equation AUC, area under the curve; 95% CI, 95% confidence interval; BOLD, blood oxygen level–dependent.
[a]Represented $P<0.05$ by comparing the AUC of perfusion fraction to that of eGFR.
[b]Denoted $P<0.01$ by comparing the AUC of BOLD to that of eGFR.
[c]Indicated that data were analyzed from all 103 patients with allograft injury.
[d]Denoted that data were analyzed from 93 patients with BOLD results.

dysfunction in preclinical animal models. Nevertheless, this modality is curtailed by radiation exposure and potentially contrast-induced nephropathy, which is a particular concern for patients with impaired graft function. Arterial spin labeling is particularly alluring given that it is radiation-free and can be performed in patients with allograft dysfunction without the need for contrast injection.

Kidney hypoxia is a potent functional rather than anatomic biomarker for interstitial fibrosis. Oxygen homeostasis plays a pivotal role in the normal function of tubulointerstitium, and disturbed oxygen equilibrium has been reported to drive fibrosis progression and reduce kidney survival (21). Several previous investigations have examined the relationship between kidney function and R2* in patients with CKD with divergent results (22,23). The results of previous studies are not directly comparable with ours because biopsy references were deficient in most studies, in addition to the lack of simultaneous kidney perfusion measurement, which has been suggested to be obligatory for the interpretation of BOLD results (24). There are reports (25,26) of no cortical R2* changes in allografts with acute rejection, potentially suggesting that inflammatory cell infiltration does not influence cortical R2*.

The main diagnoses included in this study were heterogeneous and representative, with allograft rejection and glomerulonephritides each accounting for roughly one third of the cases. More importantly, correlations between functional MRI measurements and histopathologic variables in the entire allograft injury group, in patients with rejection or patients with glomerulonephritides were similar (data not shown), suggesting that assessment of interstitial fibrosis by functional MRI would probably not be influenced by cause of allograft injury.

Although the correlations observed between functional MRI measurements and histopathologic variables were moderate to strong, there were significant interindividual variabilities of functional MRI measurements even for the same interstitial fibrosis degree. However, moderate-to-excellent diagnostic performance, as indicated by receiver-operating characteristic curve analysis, supported functional MRI (particularly arterial spin labeling) as a helpful and robust modality for the differentiation of various interstitial fibrosis categories.

In this study, functional MRI was only used to evaluate interstitial fibrosis instead of acute pathologic lesions. Therefore, this technique may be particularly useful for patients with allograft dysfunction in which interstitial fibrosis/tubular atrophy is the salient histopathologic finding. Functional MRI could also potentially be used to monitor the evolution of interstitial fibrosis in clinical trials, thus obviating repeat biopsies. Additionally, the good-to-excellent performance of functional MRI to identify allografts with interstitial fibrosis >50% suggested that it could be helpful to guide clinicians to avoid unnecessary biopsies in cases of extensive interstitial fibrosis, in which the benefits gained from biopsy may not outweigh the risks. Moreover, in selected cases of apparent clinicopathologic inconsistencies, imaging the whole allograft with functional MRI could also point to the presence of scars that may be underrepresented or overrepresented in a biopsy, thereby potentially altering management and prognostication.

The main limitation of this study include its being limited to a single center. Kidney oxygenation and perfusion have been reported to be influenced by medications (27) and hydration status (28). Although we washed out the effects of medications for at least 6 hours before MRI examinations, we cannot definitively exclude the possibility that concomitant medication usage confounded our results.

In summary, we validated that functional MRI measurements were strongly correlated with kidney allograft interstitial fibrosis. We conclude that functional MRI is a robust tool that is supported by kidney histopathology to noninvasively evaluate kidney allograft interstitial fibrosis.

Disclosures

Dr. Chen, Dr. Cheng, Dr. Liu, Dr. Wang, Dr. Yu, Dr. M.C. Zhang, and Dr. L. Zhang have nothing to disclose. The authors certify that the kidneys were procured with the consents of the donors or their family members, as appropriate. No participants included in this study received kidney transplantation from executed prisoners.

Funding

Dr. Liu is supported by National Key Research and Development Program of China grant 2016YFC0904103. Dr. L. Zhang is supported by Natural Scientific Foundation of China grants 81230032 and 81322020.

Supplemental Material

This article contains the following supplemental material online at http://cjasn.asnjournals.org/lookup/suppl/doi:10.2215/CJN.00020119/-/DCSupplemental.

Supplemental Table 1. Imaging modalities and corresponding parameters used in this study.

Supplemental Figure 1. Study flowchart.

Supplemental Figure 2. Typical example of peritubular capillary density measurement using the Aperio Microvessel algorithm. An annotation layer of tubulointerstitium was created by manually drawing areas of interest that excluded glomeruli and interstitial large vessels on digitally scanned CD34-immunostained slides. By using the Aperio Microvessel algorithm, the peritubular capillary was highlighted and related parameters could be automatically calculated.

Supplemental Figure 3. Peritubular capillary density in the normal control group and allograft injury group.

References

1. Eddy AA: Overview of the cellular and molecular basis of kidney fibrosis. *Kidney Int Suppl (2011)* 4: 2–8, 2014
2. Papasotiriou M, Genovese F, Klinkhammer BM, Kunter U, Nielsen SH, Karsdal MA, Floege J, Boor P: Serum and urine markers of collagen degradation reflect renal fibrosis in experimental kidney diseases. *Nephrol Dial Transplant* 30: 1112–1121, 2015
3. Cheng O, Thuillier R, Sampson E, Schultz G, Ruiz P, Zhang X, Yuen PS, Mannon RB: Connective tissue growth factor is a biomarker and mediator of kidney allograft fibrosis. *Am J Transplant* 6: 2292–2306, 2006
4. Morrell GR, Zhang JL, Lee VS: Magnetic resonance imaging of the fibrotic kidney. *J Am Soc Nephrol* 28: 2564–2570, 2017
5. Pedersen M, Dissing TH, Mørkenborg J, Stødkilde-Jørgensen H, Hansen LH, Pedersen LB, Grenier N, Frøkiaer J: Validation of quantitative BOLD MRI measurements in kidney: Application to unilateral ureteral obstruction. *Kidney Int* 67: 2305–2312, 2005
6. Han F, Xiao W, Xu Y, Wu J, Wang Q, Wang H, Zhang M, Chen J: The significance of BOLD MRI in differentiation between renal transplant rejection and acute tubular necrosis. *Nephrol Dial Transplant* 23: 2666–2672, 2008
7. Mao W, Zhou J, Zeng M, Ding Y, Qu L, Chen C, Ding X, Wang Y, Fu C: Chronic kidney disease: Pathological and functional evaluation with intravoxel incoherent motion diffusion-weighted imaging. *J Magn Reson Imaging* 47: 1251–1259, 2018
8. Cutajar M, Thomas DL, Hales PW, Banks T, Clark CA, Gordon I: Comparison of ASL and DCE MRI for the non-invasive measurement of renal blood flow: Quantification and reproducibility. *Eur Radiol* 24: 1300–1308, 2014
9. Cai YZ, Li ZC, Zuo PL, Pfeuffer J, Li YM, Liu F, Liu RB: Diagnostic value of renal perfusion in patients with chronic kidney disease using 3D arterial spin labeling. *J Magn Reson Imaging* 46: 589–594, 2017
10. Ren T, Wen CL, Chen LH, Xie SS, Cheng Y, Fu YX, Oesingmann N, de Oliveira A, Zuo PL, Yin JZ, Xia S, Shen W: Evaluation of renal allografts function early after transplantation using intravoxel incoherent motion and arterial spin labeling MRI. *Magn Reson Imaging* 34: 908–914, 2016
11. Vink EE, de Boer A, Hoogduin HJ, Voskuil M, Leiner T, Bots ML, Joles JA, Blankestijn PJ: Renal BOLD-MRI relates to kidney function and activity of the renin-angiotensin-aldosterone system in hypertensive patients. *J Hypertens* 33: 597–603, discussion 603–604, 2015
12. Cox EF, Buchanan CE, Bradley CR, Prestwich B, Mahmoud H, Taal M, Selby NM, Francis ST: Multiparametric renal magnetic resonance imaging: Validation, interventions, and alterations in chronic kidney disease. *Front Physiol* 8: 696, 2017
13. Li H, Liang L, Li A, Hu Y, Hu D, Li Z, Kamel IR: Monoexponential, biexponential, and stretched exponential diffusion-weighted imaging models: Quantitative biomarkers for differentiating renal clear cell carcinoma and minimal fat angiomyolipoma. *J Magn Reson Imaging* 46: 240–247, 2017
14. Loupy A, Haas M, Solez K, Racusen L, Glotz D, Seron D, Nankivell BJ, Colvin RB, Afrouzian M, Akalin E, Alachkar N, Bagnasco S, Becker JU, Cornell L, Drachenberg C, Dragun D, de Kort H, Gibson IW, Kraus ES, Lefaucheur C, Legendre C, Liapis H, Muthukumar T, Nickeleit V, Orandi B, Park W, Rabant M, Randhawa P, Reed EF, Roufosse C, Seshan SV, Sis B, Singh HK, Schinstock C, Tambur A, Zeevi A, Mengel M: The Banff 2015 kidney meeting report: Current challenges in rejection classification and prospects for adopting molecular pathology. *Am J Transplant* 17: 28–41, 2017
15. Daunoravicius D, Besusparis J, Zurauskas E, Laurinaviciene A, Bironaite D, Pankuweit S, Plancoulaine B, Herlin P, Bogomolovas J, Grabauskiene V, Laurinavicius A: Quantification of myocardial fibrosis by digital image analysis and interactive stereology. *Diagn Pathol* 9: 114, 2014
16. Prasad PV: Update on renal blood oxygenation level-dependent MRI to assess intrarenal oxygenation in chronic kidney disease. *Kidney Int* 93: 778–780, 2018
17. Odudu A, Nery F, Harteveld AA, Evans RG, Pendse D, Buchanan CE, Francis ST, Fernández-Seara MA: Arterial spin labelling MRI to measure renal perfusion: A systematic review and statement paper. *Nephrol Dial Transplant* 33(suppl_2): ii15–ii21, 2018
18. Steiger P, Barbieri S, Kruse A, Ith M, Thoeny HC: Selection for biopsy of kidney transplant patients by diffusion-weighted MRI. *Eur Radiol* 27: 4336–4344, 2017
19. Afsar B, Afsar RE, Dagel T, Kaya E, Erus S, Ortiz A, Covic A, Kanbay M: Capillary rarefaction from the kidney point of view. *Clin Kidney J* 11: 295–301, 2018
20. Ehling J, Bábíčková J, Gremse F, Klinkhammer BM, Baetke S, Knuechel R, Kiessling F, Floege J, Lammers T, Boor P: Quantitative micro-computed tomography imaging of vascular dysfunction in progressive kidney diseases. *J Am Soc Nephrol* 27: 520–532, 2016
21. Nangaku M: Chronic hypoxia and tubulointerstitial injury: A final common pathway to end-stage renal failure. *J Am Soc Nephrol* 17: 17–25, 2006
22. Inoue T, Kozawa E, Okada H, Inukai K, Watanabe S, Kikuta T, Watanabe Y, Takenaka T, Katayama S, Tanaka J, Suzuki H: Noninvasive evaluation of kidney hypoxia and fibrosis using magnetic resonance imaging. *J Am Soc Nephrol* 22: 1429–1434, 2011
23. Khatir DS, Pedersen M, Jespersen B, Buus NH: Evaluation of renal blood flow and oxygenation in CKD using magnetic resonance imaging. *Am J Kidney Dis* 66: 402–411, 2015
24. van der Bel R, Coolen BF, Nederveen AJ, Potters WV, Verberne HJ, Vogt L, Stroes ES, Krediet CT: Magnetic resonance imaging-derived renal oxygenation and perfusion during continuous, steady-state angiotensin-II infusion in Healthy humans. *J Am Heart Assoc* 5: e003185, 2016
25. Djamali A, Sadowski EA, Samaniego-Picota M, Fain SB, Muehrer RJ, Alford SK, Grist TM, Becker BN: Noninvasive assessment of early kidney allograft dysfunction by blood oxygen

level-dependent magnetic resonance imaging. *Transplantation* 82: 621–628, 2006
26. Sadowski EA, Fain SB, Alford SK, Korosec FR, Fine J, Muehrer R, Djamali A, Hofmann RM, Becker BN, Grist TM: Assessment of acute renal transplant rejection with blood oxygen level-dependent MR imaging: Initial experience. *Radiology* 236: 911–919, 2005
27. Hall ME, Rocco MV, Morgan TM, Hamilton CA, Jordan JH, Edwards MS, Hall JE, Hundley WG: Beta-blocker use is associated with higher renal tissue oxygenation in hypertensive patients suspected of renal artery stenosis. *Cardiorenal Med* 6: 261–268, 2016
28. Pruijm M, Milani B, Burnier M: Blood oxygenation level-dependent MRI to assess renal oxygenation in renal diseases: Progresses and challenges. *Front Physiol* 7: 667, 2017

Received: January 2, 2019 **Accepted:** July 11, 2019

W.W. and Y.Y. contributed equally to this study.

Published online ahead of print. Publication date available at www.cjasn.org.

See related editorial, "Imaging as a Noninvasive Tool for Evaluating Interstitial Fibrosis in Kidney Allografts," on pages 1286–1287.